

The Effect of Magnetization on Electron Heating in Low-Density Ultracold Neutral Plasmas

Ryan C. Baker,¹ Bridget O'Mara,¹ and Jacob L. Roberts¹

Department of Physics, Colorado State University, Fort Collins, Colorado 80523, USA

(Dated: 27 February 2026)

Ultracold neutral plasmas provide a useful system for studying extreme parameter regimes plasma physics in an accessible laboratory setting. The parameter space of plasma physics can be characterized in part by coupling strength and degree of magnetization. The range of achievable strong coupling is determined in part by the lowest possible temperatures that can be achieved. This work examines the early-lifetime electron heating of moderately coupled, strongly magnetized plasmas. This heating is dominated by disorder-induced heating and heating due to Rydberg atom formation. By using experimentally informed simulations, it is found that disorder-induced heating has a large influence in electron temperature well into the plasma lifetime. Additionally, the dependence of the minimum achievable electron temperature on magnetization and initial electron energy is examined. In this work, we find electron temperatures as low as $0.52_{-0.05}^{+0.10}$ K (for electron density, n_e , of $6.1 \times 10^{12} \text{ m}^{-3}$), which determines the maximum coupling strength for the measured experimental conditions.

I. INTRODUCTION

Ultracold neutral plasmas (UNPs) are useful tools for exploring extreme conditions of plasma physics in tabletop-scale laboratory settings, having been utilized since the late 1990's to better understand a variety of plasma physics phenomena¹⁻³. Two important dimensionless quantities for specifying plasma parameters are magnetic field strength, β , and the electron coupling strength, Γ . While β has more than one common definition in plasma physics⁴, for this work the definition used is that β is the ratio of the cyclotron frequency of the electrons (ω_c) to the plasma frequency of the electrons (ω_{pe}). This describes how the magnetic field affects plasma processes such as transport and collisions⁵. $\beta \sim \frac{B}{\sqrt{n_e}}$, where B is the applied magnetic field and n_e is the electron density of the plasma. Γ is the ratio of the average nearest-neighbor potential energy of the electrons to the characteristic thermal energy of the electrons in the plasma⁶. This parameter describes the degree of spatial correlation between the electrons and also characterizes the degree to which many commonly used approximations are applicable (with lower Γ indicating greater applicability)⁴. $\Gamma = \frac{e^2}{4\pi\epsilon_0 a_s k_b T_e} \sim \frac{n_e^{1/3}}{T_e}$, where a_s is the Wigner-Seitz radius and T_e is the temperature of the electrons. For subjects of interest that scale with these parameters, different plasmas can be compared even if their densities and temperatures vary significantly^{5,7-9}. In this work, we use a combined experimental and simulation method to determine electron temperatures and hence electron Γ at multiple values of β in magnetized UNPs to explore the lowest electron temperatures that can be obtained.

The UNPs used in this work have comparatively low densities ($n_e = 6.1 \times 10^{12} \text{ m}^{-3}$)^{10,11}. This fact combined with low achievable temperatures ($T_e \sim 1$ K) allows for study of moderately coupled, strongly magnetized plasmas with straight-

forwardly attainable laboratory fields (140 G). The degrees of magnetization ($\beta = 17.7$) and/or coupling ($\Gamma \sim 0.8$) make this plasma comparable to plasmas used in inertial confinement fusion¹², astrophysical plasmas^{13,14}, and non-neutral plasmas¹⁵ among others^{16,17}. The primary goal of this work is exploring the parameter space with respect to strong coupling and magnetization that can be investigated in future experiments in these plasmas. Additionally, we also investigate the formation physics of such low-density UNPs.

There are two dominant heating mechanisms expected in the early lifetime of UNPs: heating due to three-body recombination and disorder-induced heating (DIH)^{18,19}. Just after plasma creation, DIH is expected to dominate in the very early lifetime of the plasma ($1-2 \omega_{pe}^{-1}$)¹⁹. When the plasma is created, there is randomness in the electron-ion position distribution. DIH is the increase of kinetic energy in the system as the electrons move to a more ordered distribution in response to their Coulomb repulsion. After this period of DIH, three-body recombination is expected to become the dominant heating mechanism^{20,21}. Three-body recombination results from the collision of two free electrons near an ion such that one electron becomes bound to the ion while the other electron carries away kinetic energy from the first electron's binding energy, ultimately resulting in heating of the plasma^{19,22}. Three-body recombination results in the creation of a Rydberg atom, which is a neutral atom with a valence electron in a highly excited state²³. While three-body recombination is the primary driver of Rydberg atom formation in weakly coupled plasmas ($\Gamma \ll 1$), as coupling strength increases there are multi-body interactions outside of isolated three-body recombination events which can produce Rydberg atoms. These multi-body interactions change the predicted density scaling of the Rydberg atom formation rate²⁴. In this work we will refer to these various processes under the umbrella term Rydberg creation. Both DIH and Rydberg creation are predicted to be significantly reduced by increasing magnetic field strength due to electrons becoming increasingly bound to the magnetic field lines¹⁹. In addition to these two heating mechanisms, heating from stray electric fields present at UNP creation can be significant²⁵.

This article has been submitted to *Physics of Plasmas*. Copyright 2026 Authors. This article is distributed under a Creative Commons Attribution-NonCommercial-NoDerivs 4.0 International (CC BY-NC-ND) License.

UNPs are well-suited for studying the effect of these heating mechanisms in part due to their low densities, which result in smaller plasma frequencies ($\omega_{pe} = 2\pi \times 20$ MHz) and thus more experimentally accessible timescales as compared to other plasmas. This allows for easier probing of the plasma early in its lifetime. In this work, early in the plasma's lifetime will be loosely defined as after the initial electron escape post plasma creation ($\sim 125 \omega_{pe}^{-1}$, $\sim 1 \mu\text{s}$ under experimental conditions) until plasma expansion has a meaningful impact on the plasma electron temperature ($\sim 2500 \omega_{pe}^{-1}$, $\sim 20 \mu\text{s}$ under experimental conditions).

The goals of this work are to investigate how Rydberg populations and early time electron temperatures shortly after UNP formation change with magnetization and initial electron ionization energies in the early lifetime of moderately coupled plasmas. DIH and Rydberg creation limit the lowest electron temperature in a given plasma, which in turn is a limiting factor of the highest achievable electron Γ . While these heating mechanisms have been studied experimentally in unmagnetized UNPs^{7,22,26,27}, this work focuses on weakly and extremely magnetized plasmas⁵, specifically in the moderately coupled regime. In particular, we test whether substantial increases in electron magnetization can produce lower electron temperatures. To do this, Rydberg populations are directly measured experimentally (section II). The results of these experiments are used to modify and constrain a molecular dynamics simulation that is used to determine the electron temperature of the plasma (section III). By examining Rydberg populations, it is found that DIH has an important impact on the amount of heating during the plasma's early lifetime. It has been determined that large increases in the magnetic field strength did not significantly decrease the temperature of the plasma. Lastly, by utilizing initial excitation to Rydberg gasses that then transition to UNPs²⁸, electron temperatures for these plasma conditions as low as 520_{-5}^{+10} mK has been found (section IV).

II. EXPERIMENTAL METHODS

The experimental sequence starts by using laser cooling techniques to create a magneto-optical trap for ⁸⁵Rb atoms²⁹. 780 nm diode lasers excite the $5S_{1/2}$ F=3 to $5P_{3/2}$ F=4 transition for primary cooling. The atoms are then transferred to a purely magnetic anti-Helmholz trap³⁰. This magnetic trap is translated via a mechanical track to the ionization region, where the UNP is created. First, the $5S_{1/2}$ F=3 to $5P_{3/2}$ F=4 transition is excited using 780 nm diode lasers. This is followed by an ionization pulse from a tunable pulsed dye-laser with a wavelength near 480 nm. By tuning the ionization pulse wavelength, we can vary initial electron energies. We specify electron energies through a Kelvin-based unit that gives the equivalent temperature in equilibrium when the ionization energy is positive ($T_0 = \frac{hc}{1.5k_b} \left(\frac{1}{\lambda_{dye}} - \frac{1}{\lambda_{thresh}} \right)$ with λ_{dye} as the dye-laser wavelength and λ_{thresh} being the ionization threshold wavelength). Initial electron energies range from 1 K below to 1 K above the ionization threshold. After creation

there is a period of free evolution and then electron measurement. The apparatus is approximately cylindrically symmetric and all applied fields are primarily along the axial direction. "DC" (slowly varying) electric fields are applied adiabatically via a wire grid near the plasma. Radio-frequency (RF) fields are applied via a copper disk within the apparatus. Magnetic fields are applied via a multi-turn wire loop outside the vacuum chamber. Electrons are extracted from the plasma with a DC field and directed towards a microchannel plate (MCP) detector. Electron collisions with the MCP create a proportional voltage signal. That signal is amplified, an example of which is shown in fig. 1. This is referred to as the electron escape signal. For ease of analysis, the signal is integrated with respect to time (fig. 1b). A more thorough overview of the experimental apparatus can be found in references 31 and 32.

To determine the density, we use UNPs formed with initial energies above threshold ($T_0 = 3.5$ K). We apply RF pulses and find the RF frequency that resonantly drives electron center-of-mass motion³². That frequency is a function of UNP density. This provides a measurement of the spatial size of the UNP given the electron-to-MCP signal calibration and that in turn allows for a density determination based on the total electron number detected for all experimental conditions.

In fig. 1, we have divided the experiment sequence into four zones to represent different stages of the experiment. The amount of electrons that are extracted during all zones is proportional to the density of the plasma. The 780 nm excitation laser intensity is adjusted to maintain a constant initial density on average.

In zone 1 electrons are ionized or excited to Rydberg states²⁸ and allowed to freely evolve for $1 \mu\text{s}$. The ionization pulse wavelength determines the initial kinetic energy (ionized) or bound state (Rydberg) of these electrons. In this experiment, it is advantageous due to signal size to set the ionization energy just below the ionization threshold. This results in a gas made of a type of Rydberg atoms we refer to as loosely bound atoms. These atoms can become ionized through either a small external electric field or collisions. This is distinguished from the broader category of Rydberg atom, which can have binding energies at or below the kinetic bottleneck²⁴. After the ionization pulse there is a rapid evolution in the plasma. Over a few plasma periods ($(2\pi \times \omega_{pe})^{-1} = 50$ ns), interactions between particles will create a Maxwellian energy distribution in the electrons. In the case of loosely bound atoms, the electrons can still exchange energy via Coulomb force mediated "collisions" while bound. While some electrons are driven deeper into bound states, many more become ionized, which causes a cascading effect of ionization within the system. Over the range of experimental parameters measured, the fraction of loosely bound electrons at $1 \mu\text{s}$ varies from 20% to 80% of the total.

During zone 1 electrons will escape the neutral plasma, which will cause a deepening in the plasma's electron confinement until there is a significantly reduced electron escape³³. Additionally, there are stray electric fields due to patch charges. These stray fields are the dominant cause of electron escape during this time. These fields were found to be relatively constant on a many hours timescale, but drifted on

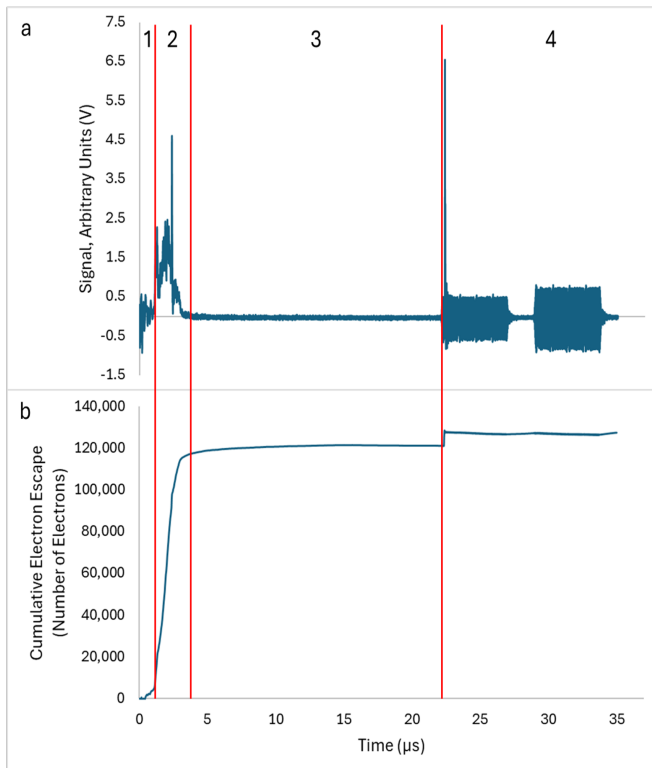


FIG. 1. Example of MCP signal (a) showing electron escape over time and the integral of that signal (b). The signal is divided into four zones as shown in the figure and described in the main text. In zone 4, there are two RF pulses applied to the plasma, evident via pickup on the MCP signal in (a), which are smoothed out via the integration in (b)

a day to day timescale. Further, there were times of rapid change, which are presumed to be due to discharges during the applied RF (zone 4). Electrodes can be used to cancel out the axial component of the stray fields. However, with the current system there is no way to cancel radial stray fields. The stray fields were measured to be less than 1 V/m for most data sets but could drift higher. For the data used to determine electron temperature limits, the stray fields were determined to be 0.65 V/m or less. To mitigate the impact of stray fields, only data taken on the same day is generally compared directly, while data taken on different days are used to establish qualitative trends. During periods of rapid change, we avoided taking data.

In zone 2 a DC field, referred to as the extraction field, is applied to remove the majority of the electrons from the plasma. This field is applied adiabatically to avoid heating the plasma. The extraction field is determined to be 13.5 V/m. This field is set to be as high as possible without distorting the MCP signal so that the free UNP electrons are extracted as quickly as possible to stop the UNP evolution. The extraction field is present for the remainder of the experiment.

In zone 3, enough time is given for any free electrons to leave the plasma, which is expanding under the effect of a Coulomb explosion and as such the free electron plasma confining potential decreases with time. Additionally, free elec-

trons on the opposite side of the plasma to the MCP can take a few microseconds to leave the plasma region. Loosely-bound Rydberg atoms are ionized by this field and their electrons escape as well.

In zone 4 an RF field is applied to ionize any Rydberg atoms that have been created. At this point the free electrons within the plasma have all left, and the remaining electrons should be bound within Rydberg atoms. RF pulses are used instead of DC fields to ionize the Rydberg atoms to ensure the best detection of the signal. In our apparatus, if a DC field from the wire grid is too large electrons can be accelerated into the wire grid instead of the detector. The use of the RF field avoids this problem as there is no net acceleration imparted to the electrons over a single RF cycle. A 40 MHz RF pulse is used to ionize the Rydberg atoms. This frequency was chosen because it resonantly couples to the electrodes around the UNP. The frequency of this RF pulse is much lower than the splitting between adjacent n quantum levels for the most bound Rydberg states that can be ionized, but the pulse amplitude is above the Inglis-Teller limit³⁴ and so there is a contribution to the signal from AC Rydberg ionization mechanisms³⁵. The sharp response in fig. 1b (at just before 23 μs) to the ionization pulse is typical, showing that Rydberg ionization is caused primarily by the leading part of the RF pulse, consistent with an effectively DC field ionization. After a brief delay, a second pulse is applied to ensure that any remaining Rydberg atoms, if present, are detected. These two pulses can be seen in the later times of fig. 1a. The amplitude of these pulses was up to 260 V/m (with a 30% uncertainty in the RF field amplitude calibration). After the Rydberg atoms are ionized, the electrons are driven to the MCP by the extraction field.

The extracted signal in zone 4 is integrated to allow a determination of the fraction of ionized electrons that became bound in Rydberg atoms as a function of initial electron temperature and applied magnetic field (section IV). The Rydberg fraction is expected to be related to the electron temperature in multiple ways. The recombination rate is predicted to be temperature-dependent^{7,24,36}. Rydberg creation produces electron heating, and so the electron temperature increases due to Rydberg atom formation. Once Rydberg atoms are formed, their states can be changed via collisions with free electrons, and that can increase or decrease the electron temperature depending on how the Rydberg atom state changes²⁴. A method for directly measuring the electron temperature in a UNP has not yet been developed for this density. Instead, we determine the electron temperature via simulations whose parameters are tuned to reproduce measured experimental results.

III. SIMULATION

A molecular dynamics (MD) code is used for the simulations. The details of the MD code can be found in references 37 and 32. Electrons and ions are treated as discrete particles and are initialized as pairs with the location of the ion being chosen randomly as described below and the elec-

tron placed 500 nm away from the ion in a random direction. The electrons and ions interact via a modified Coulomb force, $F = \frac{1}{4\pi\epsilon_0} \frac{e^2 r}{(r^2 + \alpha^2)^{3/2}} \hat{r}$, where r is the distance between particles and α is a softening parameter usually used to avoid numerical instabilities¹⁹. Starting electron velocities are oriented in a random direction with a magnitude determined by the dye-laser wavelength. The initial location of each ion is randomly determined using a Gaussian spatial distribution such that the average ion density is proportional to $e^{(-r_{ion}^2/2\sigma^2)}$ where r_{ion} is the distance from the center of the UNP and σ sets the spatial size of the UNP. The time step is $10^{-4} \omega_{pe}^{-1}$, which is small enough to achieve convergence with respect to total energy. However, it is not small enough to achieve convergence on individual particle motion such as position.

The MD is used in conjunction with the experiment. It has several parameters that are matched to the experimental measurements. The magnetic field of the MD is matched to the magnetic field of the experimental plasma. The MD density is matched to that of the experimental plasma, but the particle number is intentionally reduced to avoid the prohibitively long simulation times that a fully matched system would require. The MD results were examined as a function of particle number to confirm that there are no number dependent effects over a range of numbers similar to that used in the experiment. The stray electric fields are simulated in the MD as a constant DC field and tuned such that the percentage of electrons that are extracted in zone 1 is matched in the MD and experiment. Any heating the stray field may be providing to the electrons is accounted for in the final temperature²⁵. The MD extraction field is matched to the experiment extraction field: 13.5 V/m. As with the experiment, the majority of the electrons escape from the plasma after the extraction field is applied. Zone 3 of the experiment is modeled by a 13 μ s hold time. While this hold time is shorter than in the experiment, it was found through testing that this was long enough to get consistent results from the simulation.

The final parameter is α . As the MD is not converged with respect to individual particle motion it may not be correctly quantifying the recombination rate of the Rydberg atoms, especially those more deeply bound, which have the highest susceptibility to error as they have the highest velocities. This recombination rate can be adjusted through α to match the measured Rydberg fraction in the simulation to the experiment as a correction for imperfections of the simulation. It can do so while having a negligible effect on the DIH rate, electron collision rate, and Rydberg atoms with smaller binding energies. α also adjusts the energy distribution of the Rydberg atoms, but for the states most consistent with our observations this is a small effect, especially compared to the ultimate uncertainty of the measured electron temperature. Moreover, as will be discussed further below, the Rydberg atoms remaining after the extraction field are not significant contributors to the heating at early times and so the impact of any errors in the energy distribution are likely to be minimal with respect to the electron temperature determination. Once all these parameters are matched between the MD and experiment, the electron temperature in the plasma can be determined. The electron tem-

perature is defined by the kinetic energy of free electrons at a time of 1 μ s using the relationship $\frac{3}{2}Nk_B T_e = \sum_{i=1}^N \frac{1}{2}m_e v_i^2$, where N is the total number of free electrons and v_i is the velocity of a given free electron. Free electrons are defined as electrons that do not share the same nearest neighbor ion at both times 900 ns and 1 μ s and have not escaped due to the stray field.

The need to use α as an adjustable parameter to match the experimental observations is a subject of continued investigation. While effects such as quantum mechanics, blackbody radiation³⁸, and bremsstrahlung radiation³⁹ are not included in the simulations, they are also not expected to be significant for our UNP conditions based on simple estimates. That being said, there are experiments elsewhere that have shown both blackbody radiation-induced state-mixing for times less than 1 μ s⁴⁰ and predictions that the Rydberg state angular momentum can affect electron ionization cross sections⁴¹ and so there is a possible mechanism related to blackbody radiation leading to reduced Rydberg population. We are investigating this along with potential effects associated with the lack of convergence in electron velocity and position as future work beyond the scope of the results reported here.

IV. RESULTS

There are three trends that were explored in addition to the overall electron temperature found through the simulation: Rydberg number vs. density, Rydberg number vs. magnetic field, and Rydberg number vs. initial electron temperature. These trends should be used to better understand the electron temperatures that were found using the MD simulation.

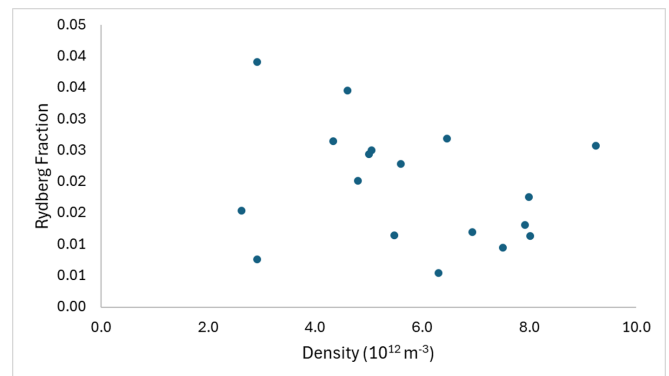


FIG. 2. A typical data set showing shot-to-shot variation in Rydberg fraction and total electron number (and thus density). Variation in the total electron number stems from variation in the loading and ionization process of the atom cloud. Variation in the Rydberg fraction stems from variation in Rydberg number from shot to shot. MCP signal background noise contributes to variation in both Rydberg fraction and total electron number measurement. In the density range that was measured, throughout many such data sets, there was no evidence of n_e^2 scaling.

Rydberg fraction versus density was analyzed using the “natural” variation between shots (fig. 2). Three-body recombination as the primary heating mechanism would predict²² a

scaling in this quantity proportional to n_e^2 . We found no strong scaling in Rydberg fraction with density as ascertained from multiple data sets like that shown in fig. 2. It has been predicted and measured that as the coupling increases into the moderate and strong regimes the $\sim n_e^2$ scaling is not expected to hold^{22,24}. Therefore, it can be reasonably assumed that this deviation from n_e^2 scaling can be attributed to the moderate coupling of the plasma.

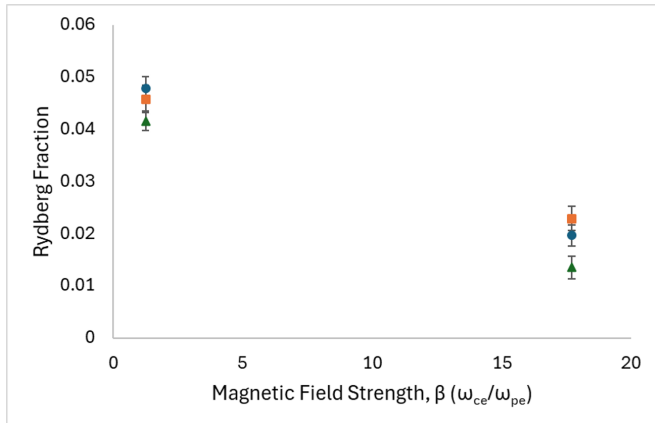


FIG. 3. Data showing the Rydberg fraction as a function of magnetic field strength β and applied RF field ($T_0 = -1$ K). The 260 V/m (blue circles) and 180 V/m (orange squares) RF amplitude sets of data have no significant difference in Rydberg fraction in most cases. This is further discussed in the main text. The 100 V/m (green triangles) RF amplitude shows a lower Rydberg fraction. This lower Rydberg fraction is indicative of a field that is insufficient to ionize all of the Rydberg atoms.

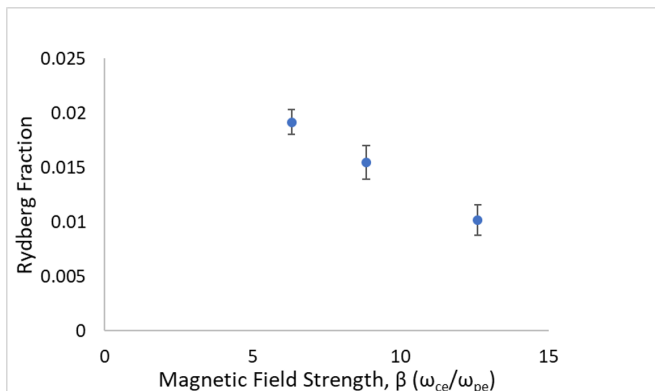


FIG. 4. Rydberg fraction vs. β for intermediate magnetic field strengths (260 V/m RF field, $T_0 = -1$ K). The purpose of this data is to demonstrate that there is no resonant or abrupt behavior in the Rydberg fraction as the magnetic field is increased. This data cannot be quantitatively compared to fig. 3 (see main text for details).

Figs. 3 and 4 show the relationship between Rydberg number and magnetic field. In these sets of experiments laboratory fields of 10 G ($\beta = 1.3$) and 140 G ($\beta = 17.7$) are compared. Fig. 3 shows a clear decrease in Rydberg population between the low and high magnetization conditions. Additional intermediate fields were also checked to ensure that there is a

smooth variation in Rydberg fraction as the magnetic field is increased, as shown in fig. 4. Due to variations in stray fields as described above, the Rydberg fractions between figs. 3 and 4 cannot be quantitatively compared. The decrease in Rydberg fraction with magnetic field strength is predicted to occur^{19,24}. Electrons in stronger magnetic fields have their directions of movement limited, as the cyclotron radius decreases and the electrons become more closely bound to the field lines, reducing the collisional Rydberg creation rate^{19,42}.

We investigated the possibility that there were Rydberg atoms that were present that we failed to detect. In fig. 3, it is shown that the measured Rydberg fraction is consistent with saturation between 180 V/m and 260 V/m RF pulses. This indicates that it is unlikely that we are missing a significant number of Rydberg atoms. This degree of saturation was present in all except the $\beta = 1.3$ and $T_0 = 0$ K case. To evaluate how many Rydberg atoms might be going undetected in that case, the time dependence of the Rydberg ionization signal in zone 4 can be used to get information about the binding energy distribution of the Rydberg atoms since less bound atoms are ionized more rapidly. To do so, ionization signals vs. binding energy in Rydberg gases with low enough density that UNPs do not form were measured experimentally. From estimates based on the time dependence of the measured ionization signals, it is unlikely that more than 20% of the Rydberg atoms went undetected. With respect to other considerations, the radiative lifetimes of the Rydberg atoms being measured are calculated to be hundreds of microseconds³⁵. Measurement of Rydberg atoms as a function of the hold time in zone 3 did not indicate any loss rates in Rydberg number that would noticeably lower the measured fraction. For the $T_0 = 0$ K, $\beta = 1.3$ condition, making comparisons to magnetic-field-free predictions of Rydberg atom formation rates seems reasonable¹⁹. In light of this, we note that there is consistency between our measured Rydberg fractions with predictions from Ref.²⁴, using the electron temperature determined by our matched MD simulation.

Lastly, fig. 5 shows the relationship between Rydberg population and initial ionization energy. As expected, the Rydberg fraction decreases both with increasing T_0 and increasing magnetic field. Signal-to-noise considerations make measurements of the Rydberg fraction at higher values of T_0 difficult. With respect to the data collected with $T_0 < 0$, although the fraction of free electrons in the plasma can depend on the initial ionization energy, there is no evidence of any threshold effects. So, there are no qualitative changes in plasma properties or evolution associated with the ionization threshold.

These observed trends contribute to a better understanding of the electron temperature results presented in table 1. Table 1 shows the electron temperatures and associated Γ early in the UNP lifetime for different combinations of initial ionization energy and magnetic field strength. The uncertainties shown in the electron temperatures are the combination of experimental uncertainties and those associated with the variance in the parameters chosen and tuned in the MD. Beginning with the $T_0 = 0$ K conditions, it is seen that increasing the magnetic field strength does not significantly increase Γ , although there is a mild dependence. Additionally, referring

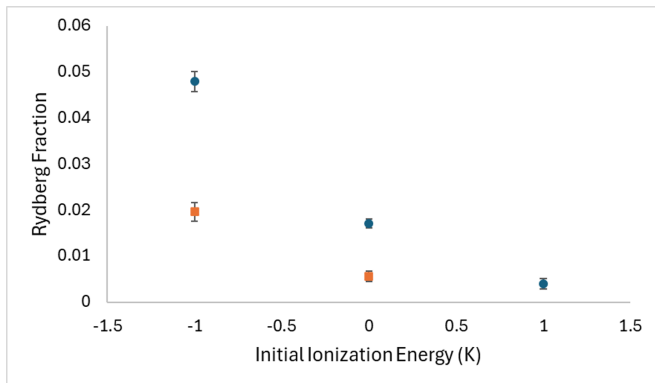


FIG. 5. Rydberg fraction vs. initial ionization energy expressed in units of equivalent temperature (see main text for details) using a 260 V/m RF field. Low magnetic field strength ($\beta = 1.3$) is represented by the blue circles. High magnetic field strength ($\beta = 17.7$) is represented by the orange squares. There is no high field point for the 1 K condition. As the temperature increases, the Rydberg fraction decreases. There is approximately a factor of 2.5 decrease in Rydberg fraction between the low and high fields in both the -1 K and 0 K cases.

β	T_0 (K)	T_e (K)	Γ
1.3	0.0	$0.90^{+.17}_{-.09}$	$0.55^{+.09}_{-.06}$
17.7	0.0	$0.68^{+.13}_{-.07}$	$0.72^{+.12}_{-.08}$
1.3	-1.0	$0.58^{+.11}_{-.06}$	$0.85^{+.14}_{-.10}$
17.7	-1.0	$0.52^{+.10}_{-.05}$	$0.95^{+.15}_{-.10}$

TABLE I. Table showing electron temperature and Γ at the end of zone 1 under different magnetization and initial ionization energy combinations.

to fig. 5, one sees that the measured Rydberg population fell by just over a factor of 2 between the low and high magnetic field strengths. This relatively small population of Rydberg atoms is not enough to account for total electron heating in the early plasma lifetime. We note that there is a population of Rydberg atoms that would be ionized by the extraction field. These electrons would be extracted during zone 2, and not included in the Rydberg population ionized by the RF pulses. Totalling all Rydberg creation heating (heating from Rydberg atoms ionized by the RF plus those ionized by the extraction field) plus the heating from any stray electric field results in an estimated amount that is less than 1/3 of the total heating derived from the experiment-matched MD simulation. This indicates that DIH represents the most significant heating contribution in the plasma's early lifetime for these conditions.

These findings are echoed in the $T_0 = -1$ K conditions, where Γ is seen to have no significant reduction with increasing magnetic field strength. This is despite the reduction in

measured Rydberg population seen in fig. 5. This reinforces that the reduction in Rydberg population due to the presence of a magnetic field does not have a significant impact on the heating of the plasma, further demonstrating the importance of DIH as a plasma heating mechanism at early times. By using an initial ionization energy just under threshold, it is possible to push Γ to a higher value than what can be achieved starting with a fully ionized plasma. However, the resulting mixture of free and loosely bound Rydberg atoms where the latter can outnumber the former presents potential complications for using such UNPs in other experiments. Similar levels of temperature reduction can be achieved by increasing magnetic field strength without the introduction of Rydberg gasses. That being said, when starting with a Rydberg gas, it was found that for these conditions the upper limit on Γ was $0.95^{+.15}_{-.10}$, with a corresponding electron temperature of 520^{+10}_{-5} mK.

V. CONCLUSIONS

We describe an analysis method for determining the early time electron temperature in an ultracold neutral plasma through a combined experimental measurement and simulation technique. This is used to study how early lifetime heating in a plasma depends on magnetization and initial temperature. We have determined that in the moderate coupling regime for our conditions, there is no observed n_e^2 scaling of Rydberg formation rate and so Rydberg atom creation does not occur primarily via three-body recombination. We also see that there is a significant dependence of the Rydberg atom number on both magnetic field strength and initial ionization energy, with a rapid decrease in number with both increasing ionization energy and increasing magnetic field strength. Despite these dependencies, we do not observe a corresponding dependencies on electron temperature, indicating the importance of disorder-induced heating for the early lifetime of ultracold neutral plasmas. Lastly, we see that the magnetic field strength has limited impact on the electron temperature, and that excitation to Rydberg gasses can be used to achieve lower electron temperatures for these plasmas.

Expanding this work further would benefit greatly from increasing the stability in the data collection procedure. To support such an effort, we plan to install electrodes to cancel the radial stray field in the system, allowing data sets taken over a longer time to be quantitatively compared. Additionally, we are investigating ways to improve our MD code to allow for smaller step sizes without unreasonable run times, which has the potential to address any convergence-related imperfections. These fixes would allow expansion of parameter space explored. Two directions of such an expansion are to take more data at the intermediate magnetic fields, which may allow for determining a functional form of electron temperature variation with magnetic field, and going to even lower initial electron energy to search for the upper bounds of Γ for our experimental conditions.

ACKNOWLEDGEMENTS

This work was funded by the Air Force Office of Scientific Research (AFOSR), grant number FA9550-21-1-0340.

AUTHOR DECLARATIONS

Conflict of Interest

The authors have no conflicts to disclose

Author Contributions

Ryan Baker: Conceptualization (supporting); Data curation (equal); Formal analysis (equal); Investigation (lead); Methodology (equal); Project administration (equal); Software (lead); Validation (equal); Visualization (lead); Writing - original draft (lead); Writing - review & editing (equal). **Bridget O'Mara:** Investigation (supporting); Validation (supporting); Writing - review & editing (supporting). **Jacob Roberts:** Conceptualization (lead); Data curation (equal); Formal analysis (equal); Funding acquisition (lead); Methodology (equal); Project administration (equal); Resources (lead); Software (supporting); Supervision (lead); Validation (equal); Visualization (supporting); Writing - original draft (supporting); Writing - review & editing (equal).

DATA AVAILABILITY

The data that support the findings of this study are available from the corresponding author upon reasonable request.

REFERENCES

- ¹M. Lyon and S. L. Rolston, "Ultracold neutral plasmas," *Rep. Prog. Phys.* **80** (2017), 10.1088/0034-4885/80/1/017001.
- ²T. C. Killian and S. L. Rolston, "Ultracold neutral plasmas," *Phys. Today* **63**, 46–51 (2010).
- ³T. Killian, S. Kulin, S. Bergeson, L. Orozco, C. Orzel, and S. Rolston, "Creation of an ultracold neutral plasma," *Phys. Rev. Lett.* **83**, 4776–4779 (1999).
- ⁴F. F. Chen, *Introduction to Plasma Physics and Controlled Fusion* (Springer Cham, 2016).
- ⁵S. D. Baalrud and J. Daligault, "Transport regimes spanning magnetization-coupling phase space," *Phys. Rev. E* **96** (2017), 10.1103/PhysRevE.96.043202.
- ⁶J. Castro, P. McQuillen, H. Gao, and T. C. Killian, "The role of collisions and strong coupling in ultracold plasmas," in *XXVI International Conference on Photonic, Electronic and Atomic Collisions*, Journal of Physics Conference Series, Vol. 194, edited by A. Orel, A. Starace, D. Nikolic, N. Berrah, T. Gorczyca, E. Kamber, and J. Tanis (CRYOGENIC Ltd; IOP; Kalamazoo Cty Convent & Visitors Bur; Natl Electrostat Corp; PhysMath Cent; RoentDek Handels GmbH; Taylor & Francis Grp; WIENER Corp; WMU, Dept Phys; WMU, Coll Arts & Sci; WMU, Off Vice President Res; WMU, Grad Coll; WMU, Diether H Haenicke Inst Global Educ, 2009) 26th International Conference on Photonic, Electronic and Atomic Collisions, Western Michigan Univ, Kalamazoo, MI, JUL 22-28, 2009.
- ⁷R. S. Fletcher, X. L. Zhang, and S. L. Rolston, "Using three-body recombination to extract electron temperatures of ultracold plasmas," *Phys. Rev. Lett.* **99** (2007), 10.1103/PhysRevLett.99.145001.
- ⁸M. Lyon, S. D. Bergeson, and M. S. Murillo, "Limit of strong ion coupling due to electron shielding," *Phys. Rev. E* **87** (2013), 10.1103/PhysRevE.87.033101.
- ⁹S. D. Bergeson, S. D. Baalrud, C. L. Ellison, E. Grant, F. R. Graziani, T. C. Killian, M. S. Murillo, J. L. Roberts, and L. G. Stanton, "Exploring the crossover between high-energy-density plasma and ultracold neutral plasma physics," *Phys. Plasmas* **26** (2019), 10.1063/1.5119144.
- ¹⁰T. Killian, M. Lim, S. Kulin, and S. Rolston, "Ultracold neutral plasmas," in *Non-Neutral Plasma Physics IV*, AIP Conference Proceedings, Vol. 606, edited by F. Anderegg, L. Schweikhard, and C. Driscoll (USN, Off Naval Res; Natl Sci Fdn; US DOE; Inst Pure & Appl Phys Sci, UCSD, 2002) pp. 96–101, workshop on Non-Neutral Plasmas, Univ Calif San Diego, San Diego, CA, JUL 30-AUG 02, 2001.
- ¹¹M. Lyon and S. D. Bergeson, "Towards stronger coulomb coupling in an ultracold neutral plasma," *Contrib. Plasma Phys.* **55**, 399–406 (2015), international Conference on Strongly Coupled Coulomb Systems (SCCS), Santa Fe, NM, JUN 27-AUG 01, 2014.
- ¹²R. Betti and O. A. Hurricane, "Inertial-confinement fusion with lasers," *Nat. Phys.* **12**, 435–448 (2016).
- ¹³H. Vanhorn, "Dense astrophysical plasmas," *Science* **252**, 384–389 (1991).
- ¹⁴B. Paxton, L. Bildsten, A. Dotter, F. Herwig, P. Lesaffre, and F. Timmes, "Modules for experiments in stellar astrophysics (mesa)," *Astrophys. J. Suppl. Ser.* **192** (2011), 10.1088/0067-0049/192/1/3.
- ¹⁵D. Dubin and T. O'Neil, "Trapped nonneutral plasmas, liquids, and crystals (the thermal equilibrium states)," *Rev. Mod. Phys.* **71**, 87–172 (1999).
- ¹⁶J. A. Frenje, P. E. Grabowski, C. K. Li, F. H. Seguni, A. B. Zylstra, M. G. Johnson, R. D. Petrasso, V. Y. Glebov, and T. C. Sangster, "Measurements of ion stopping around the bragg peak in high-energy-density plasmas," *Phys. Rev. Lett.* **115** (2015), 10.1103/PhysRevLett.115.205001.
- ¹⁷C. Paquette, C. Pelletier, G. Fontaine, and G. Michaud, "Diffusion-coefficients for stellar plasmas," *Astrophys. J. Suppl. Ser.* **61**, 177–195 (1986).
- ¹⁸S. D. Bergeson, A. Denning, M. Lyon, and F. Robicheaux, "Density and temperature scaling of disorder-induced heating in ultracold plasmas," *Phys. Rev. A* **83** (2011), 10.1103/PhysRevA.83.023409.
- ¹⁹S. K. Tiwari and S. D. Baalrud, "Reduction of electron heating by magnetizing ultracold neutral plasma," *Phys. Plasmas* **25** (2018), 10.1063/1.5013320.
- ²⁰T. Killian, M. Lim, S. Kulin, R. Dumke, S. Bergeson, and S. Rolston, "Formation of rydberg atoms in an expanding ultracold neutral plasma," *Phys. Rev. Lett.* **86**, 3759–3762 (2001).
- ²¹F. Robicheaux and J. Hanson, "Simulation of the expansion of an ultracold neutral plasma," *Phys. Rev. Lett.* **88** (2002), 10.1103/PhysRevLett.88.055002.
- ²²S. D. Bergeson and F. Robicheaux, "Recombination fluorescence in ultracold neutral plasmas," *Phys. Rev. Lett.* **101** (2008), 10.1103/PhysRevLett.101.073202.
- ²³T. F. Gallagher, *Rydberg Atoms*, Cambridge Monographs on Atomic, Molecular and Chemical Physics (Cambridge University Press, 1994).
- ²⁴G. Bannasch and T. Pohl, "Rydberg-atom formation in strongly correlated ultracold plasmas," *Phys. Rev. A* **84** (2011), 10.1103/PhysRevA.84.052710.
- ²⁵P. Jiang and J. L. Roberts, "Electric field influences on the initial electron temperature of ultracold plasmas," *Phys. Plasmas* **26** (2019), 10.1063/1.5092238.
- ²⁶A. A. Bobrov, S. Y. Bronin, B. B. Zelener, B. V. Zelener, E. A. Manykin, and D. R. Khikhlikha, "Electron distribution function and recombination coefficient in ultracold plasma in a magnetic field," *J. Exp. Theor. Phys.* **117**, 161–168 (2013).
- ²⁷P. Gupta, S. Laha, C. E. Simien, H. Gao, J. Castro, T. C. Killian, and T. Pohl, "Electron-temperature evolution in expanding ultracold neutral plasmas," *Phys. Rev. Lett.* **99** (2007), 10.1103/PhysRevLett.99.075005.
- ²⁸M. Robinson, B. Tolra, M. Noel, T. Gallagher, and P. Pillet, "Spontaneous evolution of rydberg atoms into an ultracold plasma," *Phys. Rev. Lett.* **85**, 4466–4469 (2000).
- ²⁹E. Raab, M. Prentiss, A. Cable, S. Chu, and D. Pritchard, "Trapping of neutral sodium atoms with radiation pressure," *Phys. Rev. Lett.* **59**, 2631–2634 (1987).

- ³⁰H. Lewandowski, D. Harber, D. Whitaker, and E. Cornell, “Simplified system for creating a bose-einstein condensate,” *J. Low Temp. Phys.* **132**, 309–367 (2003).
- ³¹W.-T. Chen, C. Witte, and J. L. Roberts, “Observation of a strong-coupling effect on electron-ion collisions in ultracold plasmas,” *Phys. Rev. E* **96** (2017), 10.1103/PhysRevE.96.013203.
- ³²J. M. Guthrie, P. Jiang, and J. L. Roberts, “Calibrated heating rate measurements using electric-field-induced electron extraction in ultracold neutral plasmas,” *J. Plasma Phys.* **90** (2024), 10.1017/S0022377824000114.
- ³³R. T. Sprenkle, S. D. Bergeson, L. G. Silvestri, and M. S. Murillo, “Ultracold neutral plasma expansion in a strong uniform magnetic field,” *Phys. Rev. E* **105** (2022), 10.1103/PhysRevE.105.045201.
- ³⁴D. Inglis and E. Teller, “Tonic depression of series limits in one-electron spectra,” *Astrophys. J.* **90**, 439–448 (1939).
- ³⁵M. Archimi, C. Simonelli, L. Di Virgilio, A. Greco, M. Ceccanti, E. Arimondo, D. Ciampini, I. I. Ryabtsev, I. I. Beterov, and O. Morsch, “Measurements of single-state and state-ensemble lifetimes of high-lying rb rydberg levels,” *Phys. Rev. A* **100** (2019), 10.1103/PhysRevA.100.030501.
- ³⁶T. Pohl, D. Vrinceanu, and H. R. Sadeghpour, “Rydberg atom formation in ultracold plasmas: Small energy transfer with large consequences,” *Phys. Rev. Lett.* **100**, 223201 (2008).
- ³⁷C. Witte, *Computational Modeling of Low-Density Ultracold Plasmas*, Ph.D. thesis, Colorado State University (2017).
- ³⁸V. D. Ovsianikov, I. L. Glukhov, and E. A. Nekipelov, “Rates of blackbody radiation-induced transitions from rydberg states of alkali atoms,” *J. Phys. B: At. Mol. Opt. Phys.* **44** (2011), 10.1088/0953-4075/44/19/195010.
- ³⁹S. Ichimaru, *Basic Principles Of Plasma Physics: A Statistical Approach* (CRC Press, 1973).
- ⁴⁰M. Archimi, M. Ceccanti, M. Distefano, L. Di Virgilio, R. Franco, A. Greco, C. Simonelli, E. Arimondo, D. Ciampini, and O. Morsch, “Measurements of blackbody-radiation-induced transition rates between high-lying s, p, and d rydberg levels,” *Phys. Rev. A* **105** (2022), 10.1103/PhysRevA.105.063104.
- ⁴¹D. Vrinceanu, “Electron impact ionization of rydberg atoms,” *Phys. Rev. A* **72** (2005), 10.1103/PhysRevA.72.022722.
- ⁴²F. Robicheaux, “Three-body recombination for electrons in a strong magnetic field: Magnetic moment,” *Phys. Rev. A* **73** (2006), 10.1103/PhysRevA.73.033401.